EUROPEAN ORGANIZATION FOR NUCLEAR RESEARCH
CERN - PS DIVISION

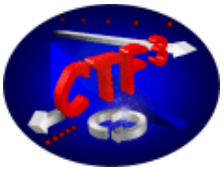

CTF3 Note 049 (MD)
PS/AE Note 2002-141
(Preliminary Phase)

Report on the operation of the CTF3 Preliminary Phase, 8 April - 24 May 2002

R. Corsini, L. Rinolfi, F. Tecker, CERN, Geneva

A. Ferrari (Ed.), Department of Radiation Sciences, Uppsala University

P. Royer, Institut de Physique des Hautes Energies, Université de Lausanne

Abstract

In this note, we report on the measurements performed on the CTF3 Preliminary Phase in the beginning of 2002. Before starting the operation with beam, hardware tests, HV conditioning of the gun and RF conditioning of the accelerating structures and of the RF deflectors were carried out. Then, measurements were performed on the front-end and on the linac in order to determine the energy, the emittance and the Twiss parameters. In the injection line, dispersion measurements were done. The beam was successfully injected and accumulated in the ring, allowing to check the optics (tune and closed orbit measurements). A summary of the results obtained during this operation period is given in this note.

Geneva, Switzerland
August 14, 2002

1 Goals

The goals for this first operation period of 2002 were to study the optics of the front-end, the linac, the injection line and the ring in both the isochronous and non-isochronous configurations, before the installation of the RF deflectors. The first two weeks were dedicated to harware tests, as well as to the HV and RF conditioning. Then, there were two periods with beam measurements, a first one between April 22 and May 3, and a second one between May 13 and May 24, in order to cross-check the results already published in [1] and to find solutions to some problems which could not be solved in 2001.

2 Conditioning of the machine and hardware tests

2.1 First week

The CTF3 machine started on April 8, according to our schedule (see Appendix), for hardware tests.

a) Magnetic measurements on the new correcting dipole WL.DBHZ36

New coils were installed inside the dipole magnet WL.BHZ36 of the spectrometer line in order to correct for the remanent field, which induces kicks on the beam. The current in WL.DBHZ36 should not exceed 10 A. Our measurements showed that the remanent field is 6.3 Gauss and that it takes about 90 s to reach this value after having switched off WL.BHZ36. With a current of 3.1 A in the correcting coils of WL.DBHZ36, the effect of the remanent field is cancelled. If the spectrometer line is used at other energies than the nominal one, i.e. if the current in WL.BHZ36 differs from 210 A, then the main dipole should be cycled at least three times.

b) Results of the alignment survey

The tilts of WL.UMA34, WL.UMA36, WL.UMA37, HIE.UMA23 and HR.UMA97 were corrected. Moreover, WL.BHZ36 and WL.MSH36 were re-aligned. The tilt and the horizontal position of the quadrupole WL.QNF352 have also been corrected.

c) Parasitic magnetic fields

At several locations in the CTF3 complex, the vacuum gauges produce a magnetic field near the beam path. For example, WL.VGP351 produces a field of 33 Gauss (resp. 3 Gauss) on the top (resp. at the bottom) of the vacuum chamber. The field experienced by the beam on its path could thus be about 15 Gauss. As for WL.VGP262, it produces a field of 22 Gauss (resp. 5 Gauss) on the top (resp. at the bottom) of the vacuum chamber. In this area of the front-end, the beam has a low energy (about 5 MeV) and it can thus be affected by these parasitic fields. Therefore, the vacuum gauges had to be moved further away from the beam pipe.

d) Test of the RF low level

Our measurements showed that the source worked fine, at the correct frequency and with the expected amplitude.

e) Test of the sextupole polarities

This check was foreseen during the first week of this commissioning period but it has been performed during the second week. The polarity of the sextupoles were found to be in agreement with the expected configuration.

f) Beam diagnostics

All beam diagnostic tools were tested according to the plans, and no major malfunction was observed.

2.2 Second week

The machine was under controlled access on April 15. A new type of patrol was required, due to the new constraints imposed by the TIS division, which is responsible for the radio-protection issues.

a) RF conditioning

The bunching system was conditioned with a power of 4 MW and a RF pulse length of 3.5 μs in MDK25. The accelerating structures ACS27 to ACS30 were conditioned with a power of 30 MW and a RF pulse length of 3.5 μs in MDK27. The accelerating structures ACS31 to ACS34 could not be conditioned because of a problem with the D'Quing system of MDK31. The RF deflectors were also conditioned, with a power of 24 MW and a RF pulse length of 1.5 μs in MDK33. However, the measured power was 6 MW in HR.SDH71 and 3 MW in HR.SDH91. After their RF conditioning, the RF deflectors were removed from the ring for the operation with beam.

b) Tests of the CLIO thermionic gun

All the electronic tests were successfully performed. The high-voltage of 100 kV was reached without any trip. The vacuum was found to be 3.2×10^{-9} Torr. Then, because of a breakdown of the Kentec amplifier and of the electronic module for the bias current, the spare pulser had to be installed in order to be able to start with beam on the following week.

3 Operation of the thermionic gun

On April 22, the operation of the CTF3 machine started with beam. Timing adjustements were performed on the CLIO thermionic gun and on the klystrons.

3.1 Setting of the CLIO thermionic gun

For the gun, the trigger pulse has been delayed by 8 RF periods, as compared to the settings used in 2001. The new setting is now KX.TGUN1 = 315. The pulse length of the gun was successfully varied between 2 and 10 ns, and the gun bias voltage was varied between -140 and -200 V. Table 1 gives the nominal values for the gun during operation.

High voltage	90 kV
Number of pulses	1 to 7
Pulse spacing	420 ns
Intensity	0.05 to 1.8 A
Maximal repetition rate	50 Hz
Heater current	1.7 A
Bias voltage	-180 V

Table 1: Nominal parameters for the gun operation.

3.2 Setting of the klystrons

The pulse spacing is 420 ns, corresponding to the EPA revolution time. With five pulses (i.e. four intervals) and with a filling time of 1.3 μs for the accelerating structures, one should have the following pulse length for the MDKs: 4 $\times$ 420 ns + 1300 ns = 2980 ns. Figure 1 shows the five pulses inside the RF pulses of MDK25 (bunching system), MDK27 and MDK31.

Figure 1: Five pulses inside the RF pulses of MDK25 (bunching system), MDK27 and MDK31.

3.3 Beam-loading measurements

During the multi-pulse operation, the effect of the beam-loading could be observed. For these measurements, the bias voltage was set to -60 V and the charge at the end of the linac was about 140×10^8 electrons per bunch. Figure 2 shows that, because of the beam-loading, the energy of the first two pulses is higher than the energy of the other pulses, as expected.

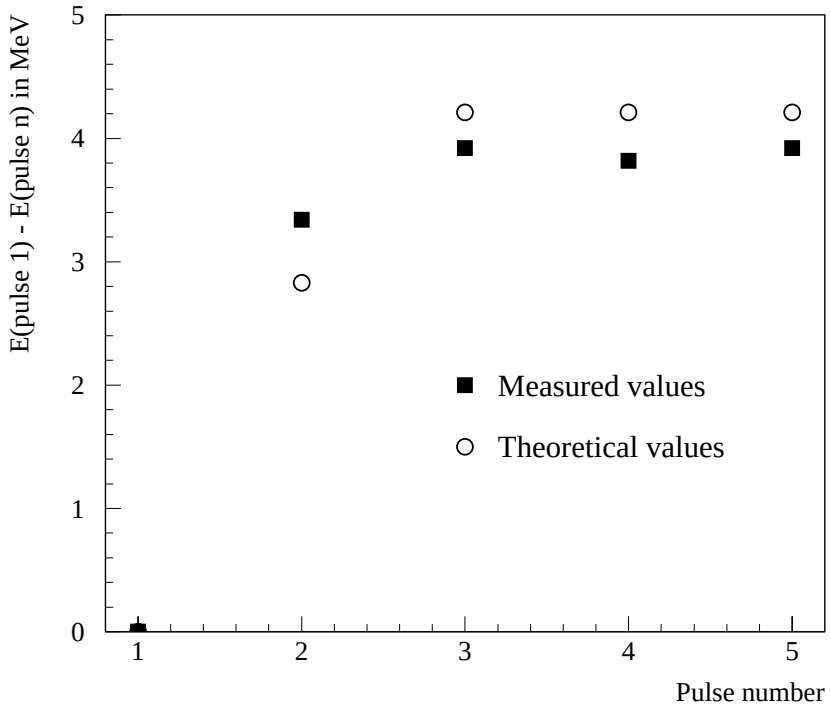

Figure 2: Measured and theoretical energy differences between the first pulse and the subsequent ones. The energy measurements were performed in the spectrometer line.

4 Beam energy measurements

During this period of the CTF3 operation, two series of energy measurements were performed, one at the exit of the bunching system and one at the end of the linac (with three different methods in that latter case).

4.1 Energy measurement at the exit of the bunching system

At the exit of the bunching system, the energy was measured by changing the current in the steering coils WL.DQSA272H and WL.DQLA27V, and by observing the corresponding position of the beam downstream in WL.UMA27. During this measurement, the power in MDK25 was 3.3 MW and the quadrupoles of the first triplet were switched off. Figure 3 shows the UMA response to the current variation for both transverse directions. The momentum was then calculated using the following excitation constants:

$$\frac{\int B\mathrm{d}l}{I} = \begin{cases} 1.14 \cdot 10^{-4}\,\mathrm{T.m/A} \\ 0.66 \cdot 10^{-4}\,\mathrm{T.m/A} \end{cases} \text{for} \begin{array}{l} \mathrm{WL.DQLA27V} \\ \mathrm{WL.DQSA272H} \end{array} .$$

This leads to a momentum of 6.7 and 6.4 MeV/c at the buncher exit, respectively. It is thus somewhat larger than what was measured in 2001.

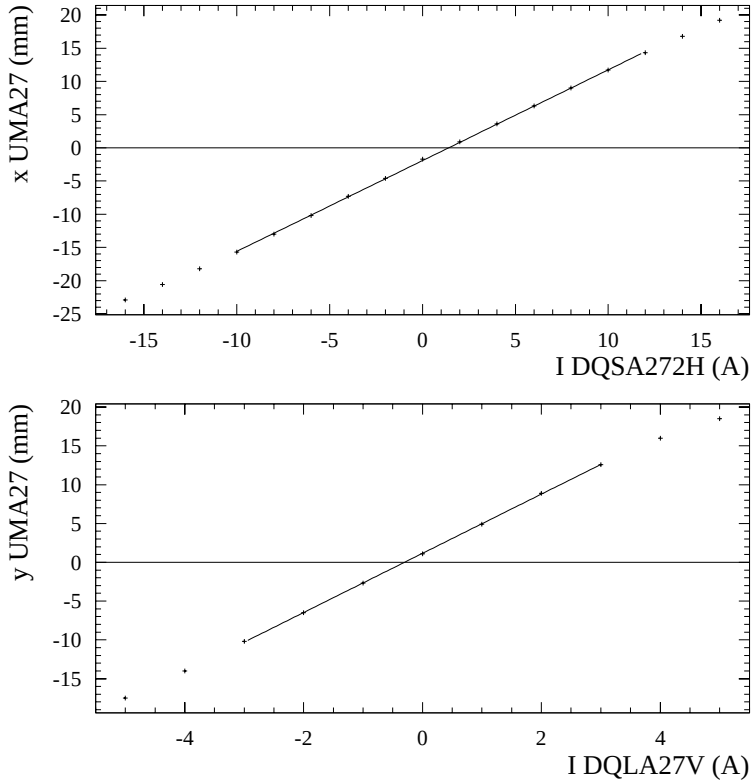

Figure 3: Horizontal and vertical beam position in WL.UMA27 as a function of the current in WL.DQSA272H (top) and WL.DQLA27V (bottom).

4.2 Energy measurement at the end of the linac

At the end of the linac, the beam energy can be measured with various methods. It can be derived from the peak power meter reading, or it can be directly measured in the spectrometer line of the matching section, or one can use the injection line as a spectrometer.

In the following, we will use the energy derived from the peak power meter reading as a reference. For each measurement point, we proceed as follows.

- first, we send the beam into the injection line, making sure that it is centered in the three TV monitors, and we record the current in HIE.BSH00.

- then, we put the beam at the center of WL.MSH36 and we record the mean energy read by the spectrometer.

- finally, we record the current in WL.BHZ36.

Knowing the calibration curves for both WL.BHZ36 and HIE.BSH00 and their deviation angle, we can derive the beam energy measured in these dipole magnets. Note that, in order to minimize the hysteresis effects, the currents in WL.BHZ36 and in HIE.BSH00 are first set to their maximal value before each measurement.

As in 2001, we observed a discrepancy between these various methods, as illustrated in Figure 4. Neither the energy measured by using the injection line as a spectrometer nor the energy measured in WL.MSH36 is consistent with the energy derived from the reading of the peak power meters. Also, we could notice that the difference between the energies measured in HIE and in the spectrometer line at the end of the linac depends on the energy range. More investigations are therefore needed.

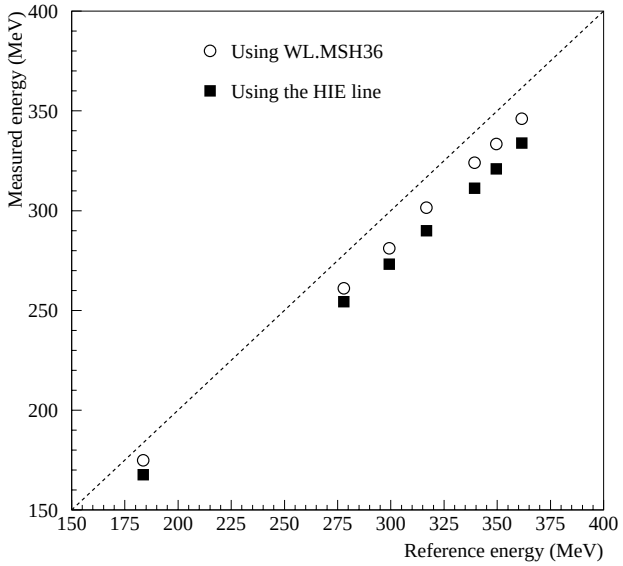

Figure 4: Energy derived from the current in HIE.BSH00 or read in WL.MSH36, as a function of the energy calculated using the peak power meter reading for MDK27 and MDK31.

5 Transverse beam dynamics

During the first period of operation with beam, some hardware tests were performed on the Wire Beam Scanners (WBS) in the linac. We observed that, when changing the current in the horizontal correcting coil WL.DQNF271H upstream of WL.WBS28, the vertical profile was displaced in WL.WBS28, thus indicating a possible inversion of the transverse directions of the wires. We also checked WL.WBS31, which was behaving as expected, and WL.WBS37. In this latter case, a few problems were discovered:

- an offset of about 5 mm was observed for the horizontal profile, while the beam was perfectly aligned up to WL.UMA37. Furthermore, when the beam was displaced from left to right in the horizontal direction with a correcting coil, we could see a displacement of the profile from right to left in WL.WBS37.

- an offset of about 1 mm was observed for the vertical profile, while the beam was perfectly aligned up to WL.UMA37. Furthermore, when the beam was displaced in the vertical direction with a correcting coil, we could see that the displacement of the profile, even if occuring in the right way, was underestimated in WL.WBS37.

In order to check the stability of the machine, a first quadrupole scan was performed by varying the current in WL.QLB29 while observing beam transverse profile in WL.WBS31. For the horizontal (resp. vertical) scan, the current in the QNFB family was set to 27 A (resp. 20 A). All beam conditions were similar to the ones used in 2001, except for the fact that the bucking coil of the gun was switched on this year. From now on, the rms beam size is obtained by fitting the transverse profile with the sum of two Gaussian distributions and by keeping only the points for which the amplitude of the signal on the wire is larger than 10% of the maximum amplitude. Figure 5 shows that the quadrupole scan performed during the first period of beam operation in 2002 is very similar to the one obtained in December 2001 [2], which ensures the stability of the machine.

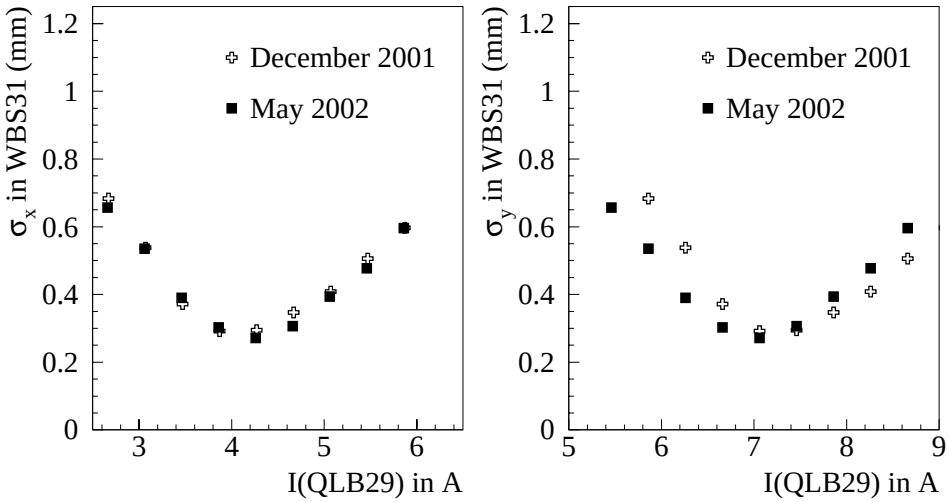

Figure 5: Transverse beam sizes in WL.WBS31 as a function of the current in WL.QLB29: the data in May 2002 are compared with the ones which were taken in December 2001.

A second quadrupole scan was performed, by varying the current in WL.QNF351 and recording beam profiles in WL.WBS37. In this case and in contrary to the measurements of 2001, all the other quadrupoles of the matching section were switched off. However, the values of the Twiss parameters and of the emittance at the entrance of WL.QNF351, as derived from this quadrupole scan, are close to the ones obtained in 2001 with similar beam conditions, see Table 2.

Lattice parameters	12 December 2001	2 May 2002
β_x (m)	18.41	15.83
α_x	-0.45	-0.83
ϵ_x (mm.mrad)	13	13
β_y (m)	31.80	23.41
α_y	-4.22	-2.92
ϵ_y (mm.mrad)	16	17

Table 2: Twiss parameters and normalised rms emittance at the entrance of WL.QNF351 derived from a quadrupole scan in WL.WBS37 performed in December 2001 [2] and May 2002.

A slight discrepancy can be observed, especially in the vertical direction. In order to match the transverse conditions at the entrance of the injection line, the currents which must be set in the quadrupoles of the section matching are those given in Table 3.

Quadrupole	Current (A)
WL.QNF351	114.45
WL.QNF352	94.68
WL.QNF353	40.35
WL.QNF371	147.38
WL.QNF372	186.87

Table 3: Currents required for a proper matching of the transverse conditions at the entrance of the injection line (MAD simulation).

6 Dispersion measurements in the injection line

Dispersion measurements were performed in the injection line, in order to check whether the experimental settings could give a dispersion pattern in agreement with the corresponding simulated optics. For this measurement, three cameras (HIE.MTV01, HIE.MTV23, HIE.MTV30), as well as two beam position monitors (HIE.UMA22, HIE.UMA23) were used. The currents in all magnetic elements were changed in order to simulate relative energy variations between -2.7% and +2.7%, while the corresponding beam positions were recorded in each diagnostic tool. Figure 6 and Figure 7 show a comparison between the dispersion curves given by the MAD model and the measured values.

In the horizontal plane, there is a very good agreement between the measured and simulated values of the dispersion at each measurement point, and the solid curve is very consistent with the points.

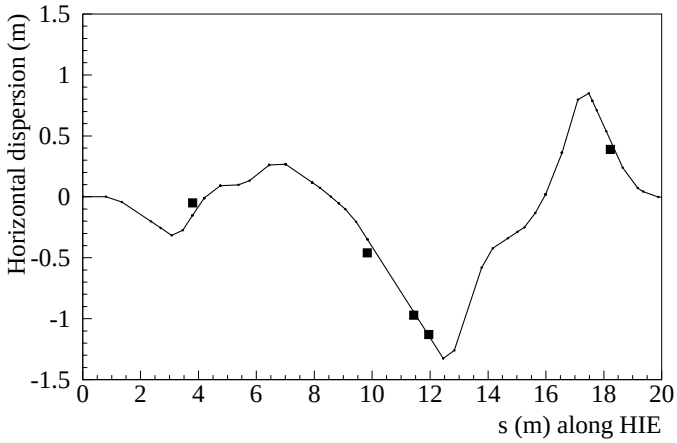

Figure 6: Horizontal dispersion measurement: the squares are the experimental points and the solid curve is given by the model for the corresponding current settings.

In the vertical plane, the discrepancy between the measured and expected values of the dispersion in HIE.MTV30 should be further investigated.

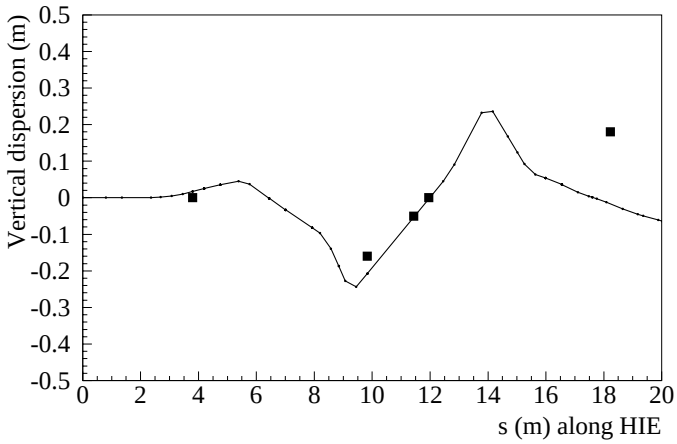

Figure 7: Vertical dispersion measurements: the squares are the experimental points and the solid curve is given by the model for the corresponding current settings. Note that the sign of the vertical dispersion calculated by MAD was inverted in order to match the measurements.

7 Measurements in the ring

7.1 Non-isochronous operation

After having adjusted the septum and the kickers for the injection and after having corrected the calibration factors of the power supplies of HR.QFN, HR.QDN, HR.XNH, HR.QFLB and HR.QFI, the first circulating beam in EPA after the 2001-2002 winter shut-down was achieved on May 16. Then, on May 21, we successfully managed to accumulate the beam (see Figure 8). For this purpose, we had to set the current in HR.BHZ to 292.3 A, which corresponds to an energy of 337 MeV, thus about 2% higher than what was measured with the injection line. This discrepancy should be better understood.

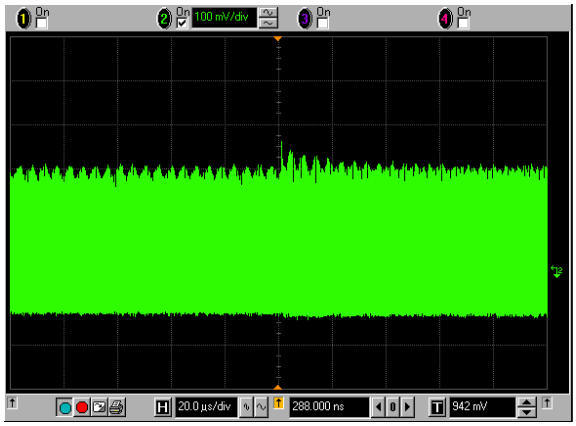

Figure 8: Accumulated beam in the non-isochronous EPA ring.

Once the beam was accumulated, tune measurements could be performed (the sextupoles were switched off). Two different methods were tested. First, we used the standard measurement system, which consists of an electrode transverse feedback system and a spectrum analyser. This system has a very long integration time and it can thus only be used with a circulating beam. Then, we tried another method, based on a Fourier Transform analysis of the horizontal and vertical signals coming from the beam position monitors of the ring (this can easily be done with a digital oscilloscope). The main advantage of this second method is that one does not need to store the beam in order to perform the tune measurement: it can thus be used with the isochronous configuration as well, in contrary to the standard measurement system. Table 4 shows the results that we obtained with each of these two methods, with an accumulated beam in the ring.

Non-integral part of the tune	Method 1	Method 2
q_h	0.915	0.916
q_v	0.455	0.443

Table 4: Measurements of the non-integral part of the tune in the non-isochronous EPA ring. Method 1 makes use of the standard measurement system. Method 2 is based on a Fourier Transform analysis of the beam position signals in HR.UMA11.

The agreement between these two methods is very good. Therefore, we have validated the method based on a Fourier Transform analysis of the beam position signals and it will be the only one that we will use in the future.

We have also compared the measured values of q_h and q_v with those obtained with the MAD model when using the experimental settings of the dipoles and the quadrupoles in the ring as input. Table 5 shows that there is a good agreement between the experimental and calculated values of the tune.

Non-integral part of the tune	Measurement 1	Measurement 2
q_h	0.89	0.95
q_v	0.44	0.43
Tune predicted by the MAD model	Measurement 1	Measurement 2
Q_h	4.93	4.96
Q_v	4.44	4.41

Table 5: Measurements of the non-integral part of the tune in the non-isochronous EPA ring and comparison with the tune values predicted when using the MAD model. In the second measurement, the current in HR.QTRB is larger by 4 A, as compared to the first measurement.

Finally, closed orbit measurements were performed at various frequencies. Figure 9 shows the horizontal measured closed orbit difference for a change in frequency from 19.089942 MHz to 19.083229 MHz. The agreement with the curve calculated with MAD by using the experimental quadrupole currents is quite good.

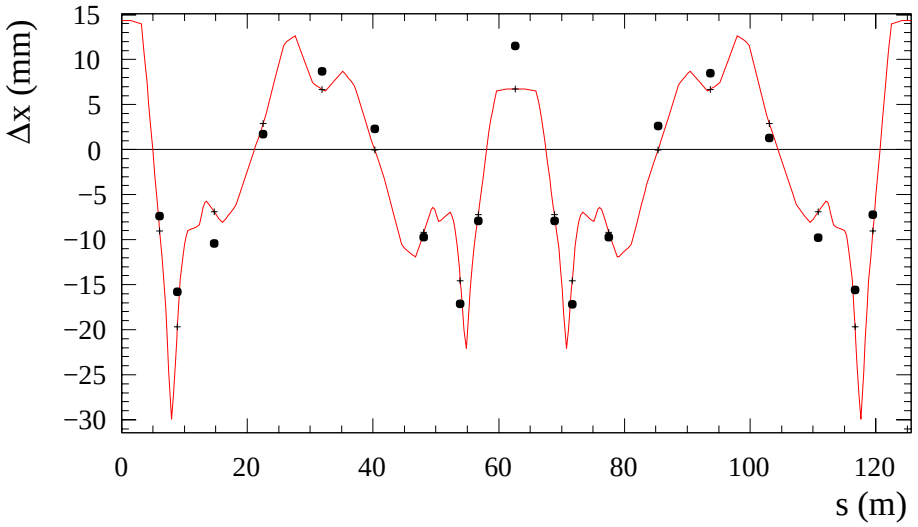

Figure 9: Measured closed orbit difference (black points) in the horizontal direction for a change in frequency from 19.089942 to 19.083229 MHz. The solid line corresponds to the expected closed orbit difference from a model with the measured currents.

Using the dispersion D_x at the UMA locations, the momentum deviation $\Delta p/p$ can be calculated from the orbit by:

$$\langle \Delta p/p \rangle = \sum_{\text{UMA}} (x \cdot D_x) \Big/ \sum_{\text{UMA}} D_x^2.$$

Figure 10 shows the calculated momentum deviation as a function of the frequency change (the closed orbit measurements were performed close to $f_0 = 19.087955$ MHz).

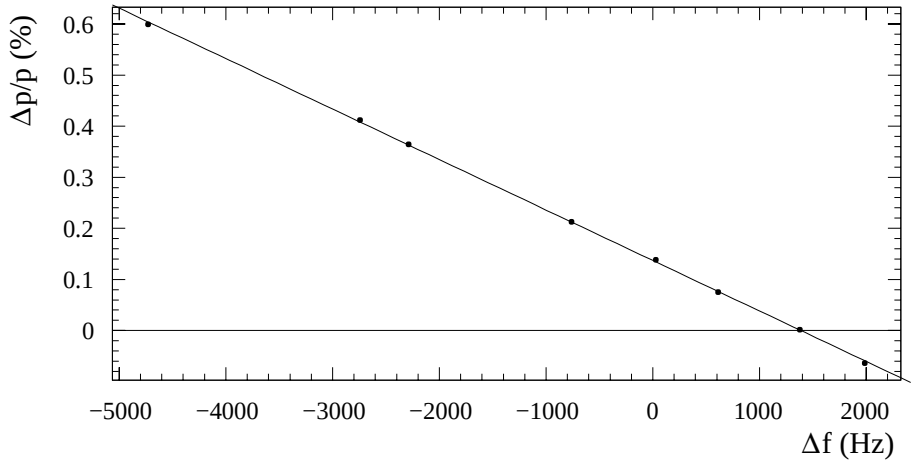

Figure 10: Calculated momentum deviation Δp/p as a function of the frequency change.

At $\Delta f = 0$, the momentum error is 0.14%. The actual closed orbit length is obtained when the momentum deviation $\Delta p/p$ vanishes, and it is found to be 125.63748 m (thus 9 mm shorter than expected). The momentum compaction factor α was calculated from the fitted slope and was found to be 0.053. This is consistent with the MAD calculation which, in this case, gives $\alpha = 0.047$.

7.2 Isochronous operation

At the end of this first operation period, the isochronous configuration of the ring was briefly tested. In particular, tune measurements based on the Fourier Transform analysis of the beam position signals were performed. A good agreement was found between the experimental values and the predictions from the MAD model, see Table 6.

Measured value of q	Q as in the MAD model
q_h = 0.78	Q_h = 4.76
q_v = 0.83	Q_v = 3.85

Table 6: Tune measurements in the isochronous EPA ring and comparison with the predictions from the MAD model.

8 Conclusion

After two weeks of hardware tests and RF conditioning, operation with beam started again in CTF3 on April 22, 2002. Within four weeks of operation, we managed to check most of the measurements performed in 2001 and we found a good consistency in our results. The linac optics is well understood but the various methods used to measure the beam energy still do not agree with each other. In the injection line, the dispersion pattern that we have obtained experimentally agrees with the predictions from the MAD model, except in the vertical direction for HIE.MTV30. The beam was successfully injected and accumulated in the ring. Tune and closed orbit measurements were performed and they both agree very well with the MAD model. The RF deflectors were installed in the machine on May 24, in order to test the bunch frequency multiplication scheme.

References

[1] R. Corsini, B. Dupuy, A. Ferrari, L. Rinolfi, P. Royer and F. Tecker, ”Commissioning of the CLIC Test Facility 3 Preliminary Phase in 2001”, CERN-PS-2002-005 (AE), CLIC note 507.

[2] D. Alesini, C. Biscari, R. Corsini, A. Drago, B. Dupuy, A. Ferrari, A. Ghigo, M. Masciarelli, L. Rinolfi, P. Royer (Ed.), M. Scampati, M. Serio and F. Tecker, ”CTF3 Preliminary Phase Commissioning, Report on Fifth and Sixth Weeks, 3-14 December 2001”, CTF3 note 044, CERN-PS/AE 2002-045.

The research of A. Ferrari has been supported by a Marie Curie Fellowship of the European Community Programme ”Improving Human Research Potentiel and the Socio-economic Knowledge Base” under contract number HPMF-CT-2000-00865.

Appendix: CTF3 operation schedule in 2002